ALMA MATER STUDIORUM
UNIVERSITÀ DI BOLOGNA

ARCHIVIO ISTITUZIONALE
DELLA RICERCA

Alma Mater Studiorum Università di Bologna
Archivio istituzionale della ricerca

Quantitative spectral electromechanical characterization of soft piezoelectric nanocomposites

This is the final peer-reviewed author's accepted manuscript (postprint) of the following publication:

Published Version:
Villa S.M., Maturi M., Santaniello T., Migliorini L., Locatelli E., Comes Franchini M., et al. (2021). Quantitative spectral electromechanical characterization of soft piezoelectric nanocomposites. SENSORS AND ACTUATORS. A, PHYSICAL, 332, 1-15 [10.1016/j.sna.2021.113196].

Availability:
This version is available at: https://hdl.handle.net/11585/846089 since: 2022-01-18

Published:
DOI: http://doi.org/10.1016/j.sna.2021.113196

Terms of use:

Some rights reserved. The terms and conditions for the reuse of this version of the manuscript are specified in the publishing policy. For all terms of use and more information see the publisher's website.

This item was downloaded from IRIS Università di Bologna (https://cris.unibo.it/).
When citing, please refer to the published version.

(Article begins on next page)

12 October 2024

This is the final peer-reviewed accepted manuscript of:
Villa S. M., Maturi M., Santaniello T., Migliorini L., Locatelli E., Comes Franchini M., Milani P. "QUANTITATIVE SPECTRAL ELECTROMECHANICAL CHARACTERIZATION OF SOFT PIEZOELECTRIC NANOCOMPOSITES" in Sensors and Actuators A: Physical, 2021, 332, 113196

The final published version is available online
https://doi.org/10.1016/j.sna.2021.113196

Terms of use:

Some rights reserved. The terms and conditions for the reuse of this version of the manuscript are specified in the publishing policy. For all terms of use and more information see the publisher's website.

This item was downloaded from IRIS Università di Bologna (https://cris.unibo.it/)

When citing, please refer to the published version.

QUANTITATIVE SPECTRAL ELECTROMECHANICAL CHARACTERIZATION OF SOFT PIEZOELECTRIC NANOCOMPOSITES

Villa S.M.; Maturi M.; Santaniello T.; Migliorini L.; Locatelli E.; Comes Franchini M.; Milani P.

Abstract

We present a modular system for the quantitative characterization of the piezoelectric coefficient of piezoelectric polymers and soft polymeric nanocomposites in the compression mode. Our approach is based on an apparatus providing spectral information on the electro-mechanical response in aselected range of frequencies of compressive loads (10–1200 Hz), with high sensitivity (down to 0.5 pC/N) and automated data acquisition modalities, enabling repeatability and reproducibility of the electro-mechanical characterization in the low-force regime (0.1 N 1.5 N). The system is modular and can be developed to cover the 2 mHz-1.2 kHz frequency range in charge mode and the 2 μHz-1200 Hz in voltage mode. We calibrated and validated the apparatus functionality using a commercial PVDF piezoelectric polymer. The suitability of the system for the quantitative measurements of the piezoelectricity of soft polymeric nanocomposites was then assessed by performing measurements of a novel piezoelectric nanocomposite material. This consisted of a polydimethylsiloxane (PDMS) matrix with embedded BaTiO3 nanoparticles, engineered with functional surface coatings to favor their homogeneous dispersion into the polymer. The proposed system demonstrated to be an effective solution for the systematic characterization of the electro-mechanical conversion properties of soft piezoelectric materials in view of soft robotics and energy harvesting applications.

1. Introduction

Soft robotics is receiving a rapidly growing interest for applications requiring close interactions with humans[1][2], biomedical active wearable and implantable devices [3][4][5] and smart sensor networks in precision agriculture [6][7]. Many of these applications rely on autonomous devices with energy production and storage, mechanosensing, and data processing capabilities [3] [4]. In this framework, the sensing and the harnessing of mechanical energy present in the ambient can represent an enabling factor for the use of for wearable or implantable devices [5].

Piezoelectric materials are an interesting solution for mechanical energy conversion via electro-mechanical coupling [3]: interesting performances have been reported for systems with mechanical properties typical of hard materials [5]. For example, the intrinsically piezoelectric polymer, Poly-Vinylidene-Fluoride (PVDF), has a piezoelectric constant of 30pC/N [8], and a Young's modulus of 2.7GPa [9]. Most of the materials constituent complex living organisms, such as skin and muscle tissue, have a modulus on the order of 10^2–10^9 Pa [10][11]. This mechanical mismatch between the common piezoelectric materials and biomechanical soft environments raise many issues linked to the absence of compliance matching [12], such as surface damages and mechanical limitation. For applications in biomedical environments softer materials are needed to minimize the interfacial stress concentration and to distribute internal loads. A widely explored solution to obtain flexible and stretchable piezoelectric materials is to combine the mechanical characteristics of a polymeric matrix with the electro-mechanical conversion property of piezoelectric nanoparticles [13][14].

In the field of piezoelectric polymeric nanocomposites many different materials are fabricated and reported [13]. the main focus is on the maximization of the piezoelectric output by varying the different ingredients (polymeric matrix, nanofiller, electrode types and other additives), unfortunately characterization techniques suitable for the quantitative measure of the piezoelectric performance of nanocomposites are still lacking [REF].

The measure of piezoelectricity presents many challenges and technical issues, caused mainly by the lack of a standard and universally recognized method [REF]. The absence of a standard set of measures that describe the performance of this type of materials, coupled with the absence of reliable methodologies to assess the classic piezoelectric constants for soft nanocomposites, results in sets of non-comparable qualitative measurements of different quantities under often unreproducible mechanical stimuli [REF] [REF]. In fact, most of the work presented in literature report operative values of voltage and current as a performance assessment, usually without a detailed description of the experimental method used to obtain them. Only for few piezocomposites the value of the piezoelectric coefficient d_{33} is presented, usually measured with a commercial system operating at a single frequency and with a single pre-load force [REF], while this class of materials has usually lower d_{33} than that of PVDF [REF] and present a non-trivial dependency to the stimuli frequency, due to the complex electro-mechanical coupling mechanism [REF][REF]. Due to these sensitivity issues these systems are usually employed to measure the piezoelectric coefficients of PVDF-based

nanocomposites [15] or piezoelectrects, namely voided charged polymers [13], which have a high piezoelectric constant, even though they lack in thermal stability, they age at high deformations and they don't show any longitudinal piezoelectric effect [16]–[19]. There is only one case of a measure of d33 concerning a piezoelectric nanocomposite with a polymeric base different than PVDF [20], where the measure was performed applying specific loads orthogonal to the substrate, and the charge was measured using an in-home built electrical conditioning circuit. The obtained piezoelectric coefficient for the nanocomposite presented is 40pC/N, but the electronic circuit has been used in a non-appropriate way, since, as will be explained in Section 2.1 the charge amplifier circuit has a lower cut-off frequency between the charge amplifying behavior and the voltage amplifying behavior, and the measure in [20] was performed with static loads, below the threshold frequency.

In this work we present an experimental set-up that allows to perform a thorough electro-mechanical characterization of the compression mode, not only in terms of quantitativeness and reproducibility of the measure even for softer piezoelectric materials which need a higher sensitivity, but also in terms of spectral distribution of the electro-mechanical conversion capabilities of this kind of material. In particular the presented experimental set-up allows to perform a quantitative and reproducible measure of the piezoelectric coefficient spectrum over a selected frequency range for piezoelectric polymeric nanocomposites with a piezoelectric coefficient d_{33} down to 0.5pC/N. The technique was validated on a commercial sample of PVDF, and then used to characterize the piezoelectric performance of a novel piezoelectric polymeric nanocomposite composed of a PDMS matrix and surface functionalized BaTiO3 nanoparticles.

2. Experimental Section

2.1 Instrument design

As stated in the introduction we need an instrument able to perform reliable and quantitative measurements of d_{33} for soft and piezoelectric nanocomposites at different frequencies, under controlled testing conditions. In order to do so this system requires a high sensibility (at least 1pC/N) and an accurate control over the mechanical stimuli amplitude, frequency, and waveform. For application purposes the most interesting regime is the low force stimuli (0.1-1N), which requires the capability of measuring charges under 1pC in order to reach said sensitivity.

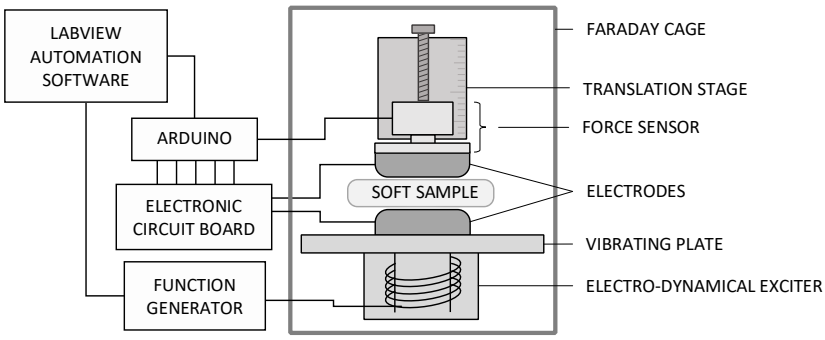

Figure 1: Experimental set-up used to measure the piezoelectric coefficient spectra of the piezoelectric polymer nanocomposite.

The system is designed to operate in a quasi-static or dynamic regime, in the way of the Berlincourt technique [21]. A vertical oscillating force is applied perpendicularly to the sample by means of an electromechanical exciter, while the force is measured by a force sensor and the output charge is collected by a dedicated electronic circuit. The system is modular, and its components can be interchanged to select different measurement ranges. The selection of an appropriate exciter and a matching force sensor allows to explore different frequency and force ranges, in this work we used a Visaton EX 60S loudspeaker and a TE Connectivity FS2050-000X-1500-G force sensor, which has a range of 14.7N and an accuracy of $\pm 1\%$. These two components allow to explore the range 0.1N-7N for the force signal amplitude and from below 1μHz up to over 1200Hz for the signal frequency. Both components are mounted on a structure appropriately designed to maintain the various elements aligned and positioned inside a Faraday cage to avoid cross-talking with electromechanical noise from the environment. The force sensor and the electro-dynamic exciter are equipped with suitable lightweight electrodes fabricated with Aluminum and electroplated with gold in order to avoid dielectric layers that would introduce spurious double-layer capacitances that interfere with the charge measurement. The force and charge electronic signals are collected and converted by an Arduino Mega ADC, and then analyzed by a dedicated LabView program. The pre-load force can be selected manually by regulating a micrometric screw gauge, and the system allows to select the stimuli frequency and the dynamic force

programmatically through the LabView software, allowing to perform multiple measurements. This allows to reproduce the measurement procedure in a very simple way by defining a measurement protocol.

A single measure is performed by imposing for every frequency of interest a sequence of oscillating force stimuli with increasing dynamic force. The charge response of the material is collected through the electrodes and converted to a voltage signal through the dedicated electronic circuit. The voltage signal is converted to a charge value using the calibration parameters found during the calibration procedure. The LabView dedicated software analyzes the force and charge signals and computes the amplitudes and the phase shift between the two signals. For every frequency $d_{33}(f)$ is calculated as the slope of the force-charge curve, so that a piezoelectric coefficient spectrum is obtained.

The core of the instrument is the dedicated electronic circuit that allows to perform the measure of the output charge from the piezoelectric element. The signal conditioning, schematized in Figure 2, is a charge amplifier circuit with some alterations to the classic layout, introduced in order to filter out the DC signal coming from the natural polarization of the samples and avoid spurious charges' integration. A typical charge amplifier circuit is an operational amplifier with a feedback loop composed of a capacitor and a resistor in parallel. The high input impedance of the operational amplifier forces the charge to accumulate over the feedback capacitor. The output voltage is therefore equal to the voltage across this capacitor, which means that the input charge can be obtained as:

$$Q_{input} = V_{output} \cdot C_F$$

This implies that the feedback capacity and the ADC set both the instrument sensitivity and range. In order to be able to read charges as small as fractions of picocoulombs we need feedback capacitors as small as 1pC, which is also the magnitude of the stray capacities for a printed circuit board. These stray capacities not only enhance the noise, but, since they are parallel to all the elements (Figure 2), they also affect the gain by a factor $1 + \frac{C_{stray}}{C_f}$, which is not negligible since C_{stray} and C_f are comparable quantities. In order to diminish the electromagnetic noises picked up by the loops and to reduce as much as possible the stray capacities, our circuit board was equipped with a ground plane, and the layout was designed in order to minimize the distances between the components.

ha eliminato: Figure 2

ha eliminato: Figure 2

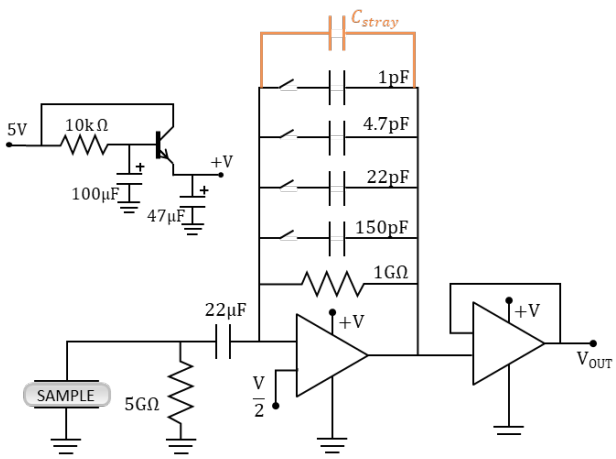

Figure 2: Charge amplifier circuit schematic with the stray capacitance that affects the gain.

In this configuration the circuit behaves as a current integrator. For real amplifiers, any input bias current causes a saturation of the signal in a very short time. To avoid this a feedback resistor is added in parallel with the capacitor, in order to discharge the capacitor periodically. Due to this addition the whole circuit has a lower cut-off frequency at:

$$f_{low} = \frac{1}{2\pi R_F C_F^*}$$

Above f_{low} the circuit behaves as a charge amplifier, while below this limit the feedback loop behaves like a resistance, which means that the circuit works as an inverting amplifier circuit with gain $A = \frac{R_f}{R_{in}}$, where R_{in} is the input impedance of the circuit. In our case the input bias capacitor, in addition to filter out the DC signals, prevents this, raising the input impedance and reducing the voltage amplifier contribution to the output signal.

In order to obtain quantitative results, the electronic circuit was calibrated using a charge input signal obtained through an AC current, controlled in amplitude I_0 and frequency f, generated with waveform generator (Agilent 32210A) coupled in series with a bias capacitor, so that the input AC signal is integrated on the capacitor becoming an oscillating charge ($Q_{in} = I_0/2\pi f$), which serves as an input for the electronic signal

conditioning circuit, which reads it as $Q_{in} = \Delta V C_F$ (Figure 3a). The calibration procedure was necessary to assess the effect of both the percentual charge loss due to contact resistance at interconnections between components and to evaluate the stray capacitance responsible for the error on the circuit gain. These contributions result in a linear loss factor, which we represented with a parameter α. We calibrated the circuit for different frequencies, using four different feedback capacities, and the results are summarized in Figure 3b. The loss parameter decreases with increasing frequency and for higher feedback capacities: this behaviour reflects the stray capacitance in parallel with the feedback capacitor and the gain behaviour near the low cut-off frequency f_{low} of the charge amplifier circuit.

ha eliminato: Figure 3

ha eliminato: Figure 3

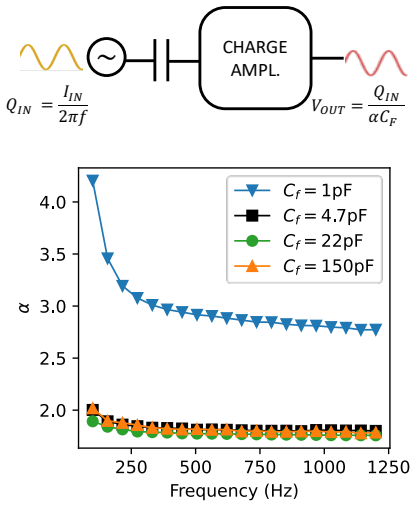

Figure 3: a) Experimental set-up for circuit calibration. b) Through the calibration procedure the loss parameter caused by the stray capacitances and the linear resistances is measured. As expected, this parameter decreases

with increasing frequency and is significantly higher for the lower feedback capacity, since it has the same magnitude of the stray capacitance.

2.2 Nanoparticle synthesis and characterization

Synthesis of tetragonal $BaTiO_3$ NPs

Barium titanate nanoparticles ($BaTiO_3$ NPs) have been synthesized according to the literature with small modifications. [DOI: 10.1111/j.1551-2916.2006.01056.x] In a typical procedure, 938 µL of titanium tetraisopropoxide (900 mg, 3.17 mmol) have been dissolved under inert atmosphere in 1.5 mL of isopropanol at room temperature in a 5 mL round-bottomed flask 2 equipped with a magnetic stirrer. Then, 1 g of $Ba(OH)_2 \cdot 8\ H_2O$ (3.17 mmol) was added, and $BaTiO_3$ NPs have been allowed to form by heating up to 80°C in 30 min and leaving the solution at 80°C for 1 h. After the reaction cooled down to room temperature, the obtained nanoparticles were centrifuged (15 min at 6000 rpm) and repeatedly washed with H_2O to remove solvent and by-products. Finally, $BaTiO_3$ NPs have been dried under vacuum to afford a fine white powder stored under inert atmosphere to avoid the formation of carbonates on the surface.

Synthesis of Dopamine Dodecylamide (DDA)

In a 500 mL round-bottomed flask equipped with a magnetic stirrer and under nitrogen flow, 2.49 g (13.2 mmol) of dopamine hydrochloride are dispersed in 100 mL of dry THF, then 4.5 mL of triethylamine (32.3 mmol) are added leading to the dissolution of dopamine. The mixture is cooled to 0°C with an ice bath and a solution of lauryl chloride (3.00 mL, 13.0 mmol) in 150 mL of dry THF is added dropwise in 3 hours. After complete addition of the acyl chloride, the mixture is stirred at room temperature for 45 minutes then 25 mL of water are added to ensure the dissolution of the precipitated triethylammonium chloride, the organic solvent is removed by rotary evaporation and the aqueous phase is extracted 3 times with ethyl acetate. The organic phase is then dried over dry Na_2SO_4 and concentrated under reduced pressure to afford DDA as a white solid. Yield = 85%. The product underwent NMR and ESI-MS analysis to assess purity and to confirm the structure (**Figure x1**). ^{1}H NMR (600 MHz, $CDCl_3$) δ = 6.77 (d, *J* = 8.0 Hz, 1H), 6.70 (d, *J* = 2.0 Hz, 1H), 6.51 (dd, *J* =

8.0, 2.0 Hz, 1H), 5.67 (t, J = 6.0 Hz, 1H), 3.45 (t, J = 7.0 Hz, 2H), 2.66 (t, J = 7.0 Hz, 2H), 2.13 (t, J = 7.0 Hz, 2H), 1.56 (m, 2H), 1.22 (bs, 16H), 0.85 (t, J = 7.0 Hz, 3H). ^{13}C-NMR (75 MHz, $CDCl_3$): δ = 14.10, 22.67, 24.80 25.7, 29.18, 29.28, 29.32, 29.45, 29.59, 31.9, 34.8, 36.8, 41.0, 115.2, 115.5, 120.4, 130.4, 143.2, 144.4, 174.7. ESI-MS [M+Na] = 358.

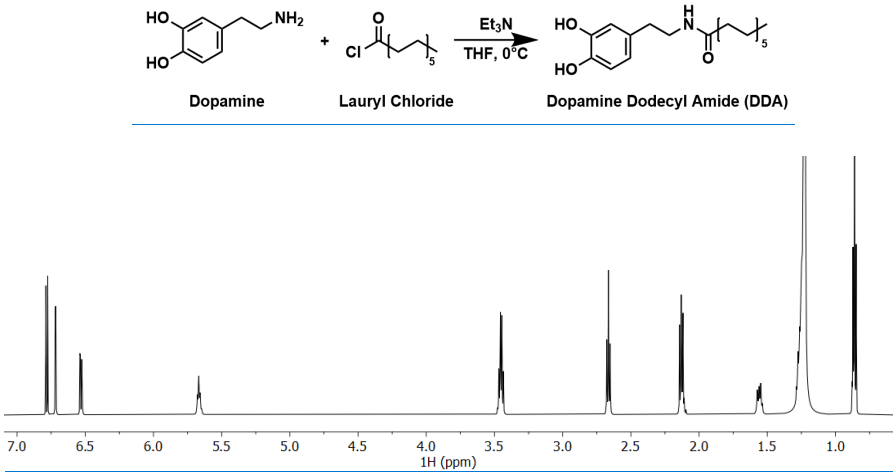

Figure x1 – Reaction scheme for the synthesis of the lipophilic DDA ligand and ^{1}H-NMR spectrum of the ligand.

Ligand exchange on BaTiO3 NPs surface

The reactive surface of $BaTiO_3$ NPs has been covered with dopamine dodecylamide (DDA) by exploiting the catechol functionality of the ligand. In a 250 mL beaker, 0.577 g of $BaTiO_3$ NPs have been redispersed in 50 mL of absolute ethanol. In order to ensure complete disaggregation of the NPs, the suspension has been treated with tip-probe sonicator (70% amplitude) for 1 min. Then, 1.15 g of DDA have been added to the suspension, which has been further ultrasonicated for another 1 min. Hence, the mixture has been placed in a 100 mL round-bottomed flask and stirred at 60°C overnight to ensure the ligand exchange.

Purification of the final mixture is performed by repeated centrifugation (15 min at 6000 rpm) and wash with ethanol two times then with hexane until colourless supernatant is obtained. Finally, the obtained $BaTiO_3$-

DDA NPs have been collected in 5 mL of hexane, leading to a uniform brown suspension of NPs. After ligand exchange reaction, the particles showed dispersibility in organic solvents such as chloroform, dichloromethane and THF.

Electron microscopy analysis

The solution is drop casted a perforated carbon film supported by a copper grid. The preparation was then dried at 100 °C. The Transmission Electron analyses were performed with a FEI TECNAI F20 microscope operating at 200 keV. The instrument is also equipped with a dispersion micro-analysis of energy (EDS) and the STEM accessory. The TEM image were taken in the phase contrast mode and Selected Area electron diffraction (SAED). STEM pictures were recorded using an High Angle Annular Dark Field (HAADF) detectors: in this imaging mode the intensity I is proportional to $Z^{1.7}t$, where Z is the mean atomic number and t is the thickness of the specimen

2.3 Nanocomposite fabrication

ha eliminato: 2

In order to achieve a uniform distribution of BaTiO3-DDA nanoparticles inside the PDMS matrix, a common organic solvent was used to dissolve the elastomer base and to disperse the nanoparticles, and the two solutions were mechanically stirred together. After the complete evaporation of the solvent, when the nanoparticles are well dispersed in the PDMS base, the curing agent is added and mechanically stirred with the PDMS-nanoparticle dispersion [22].

The fabrication procedure followed is reported below.

1. The silicon elastomer base is solved in chloroform, and the solution is mechanically stirred for 30 minutes.
2. The chosen quantity of nanoparticles is dispersed in chloroform. The mixture is mechanically stirred for 30 minutes.
3. The solution of silicon elastomer base and the nanoparticles dispersion is mixed and stirred for 20 minutes with a magnetic anchor.

4. The solution is heated at 60°C in order to speed up the solvent evaporation process. The complete evaporation of chloroform leaves the $BaTiO_3$-DDA nanoparticles dispersed in the polymer base.
5. The curing agent is added, and the mixture is mechanically stirred for other 20 minutes.
6. The obtained mixture is degassed and poured in a prepared mold.
7. The mold is degassed in a vacuum chamber in order to eliminate air bubbles trapped in the mixture during the previous phases and other bubbles originated from the roughness of the mold.
8. The material is cured at 150°C for 2,5 hours in a pre-heated oven.

In order to characterize the nanocomposite piezoelectric performance samples at different BaTiO3-DDA concentrations were produced, in particular samples with 0%, 5%, 10%, 15% and 20% nanoparticle loadings (named respectively PP5, PP10, PP15, PP20). The samples were cut into 16mm-diameter discs (Figure 4). A pristine PDMS sample (PP0) was used as a reference, in order to recognize eventual additional contributions to the electro-mechanical effect different than the piezoelectric one [23], for example the triboelectric effect [24], electrostriction [25] or dielectric charging [17].

ha eliminato: Figure 5

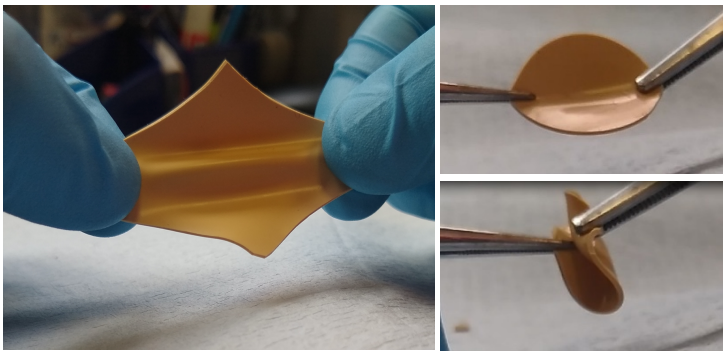

Figure 4: The PDMS-$BaTiO_3$ nanocomposite is a flexible and stretchable solid.

In order to align the electrical dipoles within the ferroelectric domains of the nanoparticles and among different nanoparticles, enhancing the piezoelectric effect [15]. In order to efficiently align the dipoles and the ferroelectric domains, a common procedure is to heat the material over its Curie temperature, and let it cool down under the action of an external electrical field (field-cooling). In order to prevent ionization discharges

in air the whole process is performed inside a vacuum chamber at the pressure of $3 \cdot 10^{-5} bar$. All the samples were poled with under the same conditions, except for control samples that were not poled in order to assess the poling effect on the piezoelectric performance of the nanocomposite.

The poling procedure is the following:

1. The samples are placed between two metal plates, forming a plane capacitor in contact with both sides of the samples.
2. The plates are heated at 130°C through resistive heaters.
3. Once the plates reach the temperature, a voltage difference of 1.2kV is imposed between the two plates, generating an electrical field of 20kV/cm. The system is kept in this configuration for 2 hours.
4. The temperature is slowly decreased from 130°C to 110°C, under the electrical field mentioned before. This first cooling phase takes two hours.
5. The heaters are turned off, and the samples cool from 110°C to room temperature under the effect of the electrical field. This second cooling phase takes another 2 hours.
6. The electrical field is turned off.

2.4 Mechanical tests

ha eliminato: 2

In order to assess quantitatively the mechanical behaviour of the nanocomposite a few mechanical measurements in a strain-stress configuration were performed, using a SAUTER Electric Test Stand with an SAUTER F50 dynamometer. The tests were performed on 24mm x 7mm x 0.6mm samples. For each sample 100 cycles of uniaxial tensile tests with a maximum deformation of 75% and a nominal velocity of 10mm/min were performed, in order to obtain the stress–strain curve and the Young's modulus at low strains, and to investigate the mechanical behaviour repeatability and any fatigue effects. The last test was carried to mechanical failure in order to measure the ultimate tensile strength of the nanocomposite material.

3. Results

The crystal structure of the prepared $BaTiO_3$ nanopowder was assessed by powder XRD giving identical results to the ones already reported by our groups in a previously published paper. [doi.org/10.1021/acsmacrolett.8b01011]. Similarly to that case, the XRD peak broadening due to the small crystallite size of the nanopowder did not allow for the assessment of the tetragonal crystal phase of $BaTiO_3$ nanoparticles.

After ligand exchange reaction (**Figure x2**) the $BaTiO_3$-DDA nanosystem showed good dispersibility and colloidal stability in organic solvents such as hexane, chloroform and THF, revealing the effectiveness of the surface modification with the synthetic catechol ligand.

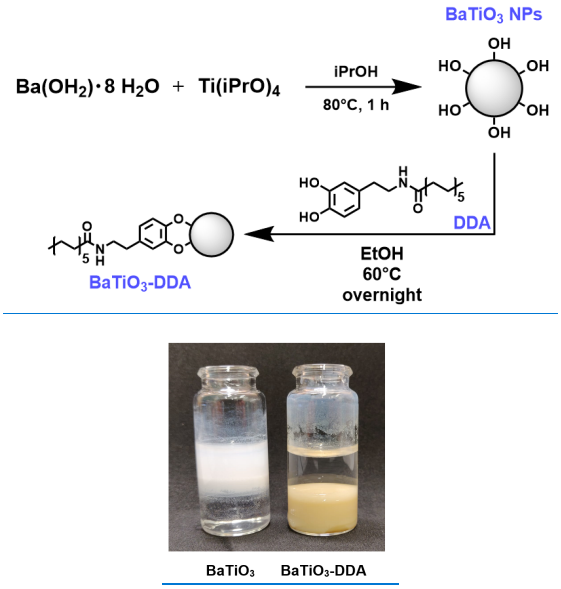

Figure x2 – Top: reaction scheme for the of lipophilic barium titanate nanoparticles by coating with dopamine dodecyl amide (DDA). Bottom: optical camera picture demonstrating the efficient stabilization of $BaTiO_3$-DDA nanoparticles in chloroform. While pristine $BaTiO_3$ nanoparticles (left) are efficiently dispersed in the upper aqueous phase and do not diffuse into the lower organic layer, lipophilic $BaTiO_3$-DDA nanoparticles show better dispersibility and inverse solubility properties.

The obtained nanosystem was therefore deeply studied by TEM analysis which first revealed the presence of crystallites having a size between 20 and 50 nm (**Figure x3**). The organic coating was also visible from TEM images as a thin layer that wraps the surface of the entire nanoparticles.

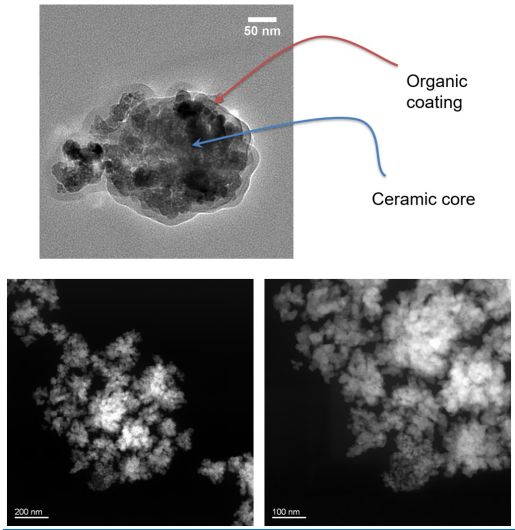

Figure x3 – TEM (top) and STEM (bottom) images of the prepared $BaTiO_3$-DDA. The organic coating is visible in TEM mode as casing the ceramic cores.

Moreover, selected-area electron diffraction (SAED) analysis was performed over a 200 nm^2 area of the sample, revealing some crystal plane reflections (**Figure x4**). Then, by software manipulation of the SAED pattern, it was possible to extract a pseudo-diffraction spectrum where the *x*-axis is attributed to the reciprocal of the distance between crystal planes. The contribution from the amorphous organic coating can be assigned to the diffuse light from the centre of the SAED pattern while the clear spots represent well-distinct crystal plane reflections. At this point, the position and relative intensities of the SAED diffraction peaks were extracted from the pseudo-diffractogram and compared to the literature values for tetragonal $BaTiO_3$

reflections, giving a good degree of match between the two. As well as for XRD analysis, the small crystallite size does not allow for the analytical determination of the degree of tetragonality of the prepared nanopowder. However, the piezoelectric properties that will be shown next reveal good piezoelectric response (and thus high tetragonality) of the nanopowder.

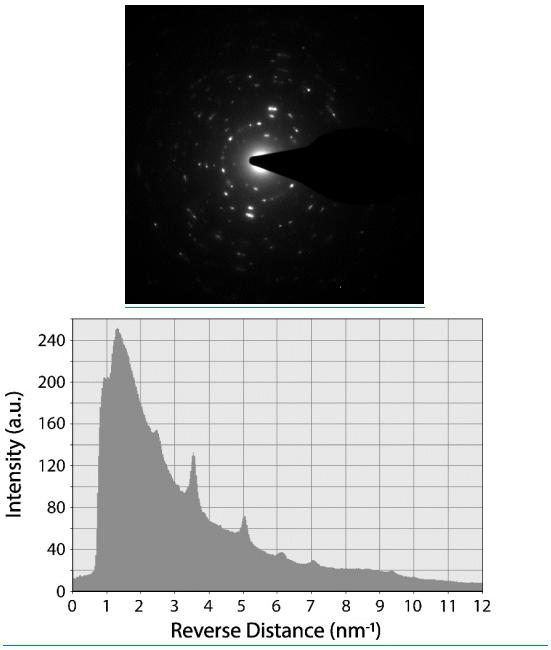

Figure x4 – TEM analysis. Top: selected-area electron diffraction (SAED) pattern of a crystalline $BaTiO_3$ nanoparticle. Bottom: integrated spectrum revealing main diffraction peaks obtained by the SAED analysis.

Finally, the elementary chemical composition of the nanopowder was assessed by energy-dispersive x-ray spectroscopy (EDX) (**Figure x5**). The irradiation of the sample by high-energy electron cause for the formation of inner electron vacancies in the specimen atoms, which then relax emitting characteristic x-ray lines that can be unambiguously attributed to the element that generated them. The Ba and O peaks are displayed. The Ti K-peak is superimposed on the Ba L-lines, but it is possible to confirm the presence of titanium by observing the

presence of the Ti L-line to the left of the oxygen peak, just above the background. The Cu characteristic line are due to the support grid.

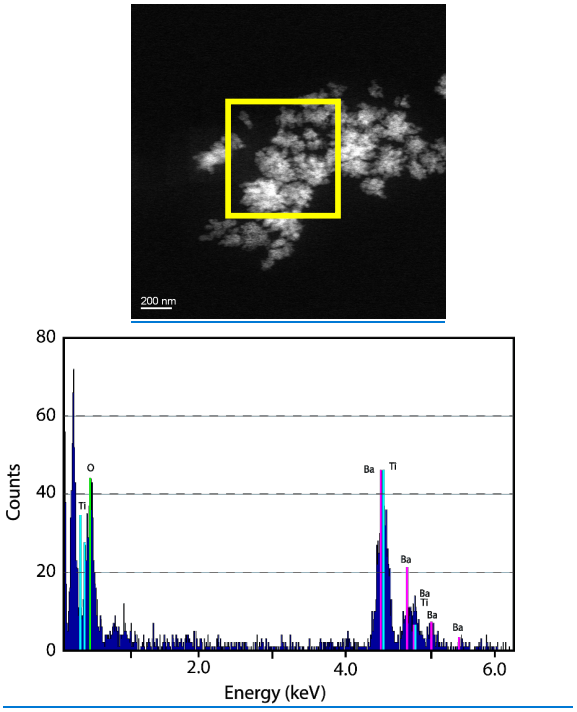

Figure x5 – Energy-dispersive x-ray spectroscopy (EDX) of the region highlighted by the yellow box in the upper STEM image. Tabulated spectral lines for barium (pink), titanium (blue) and oxygen (green) are reported for comparison.

The measuring system was validated measuring the piezoelectric coefficient spectrum of a known sample, i.e. a commercial PVDF membrane (© Precision Acoustics, thickness 110µm). The results can be observed

in

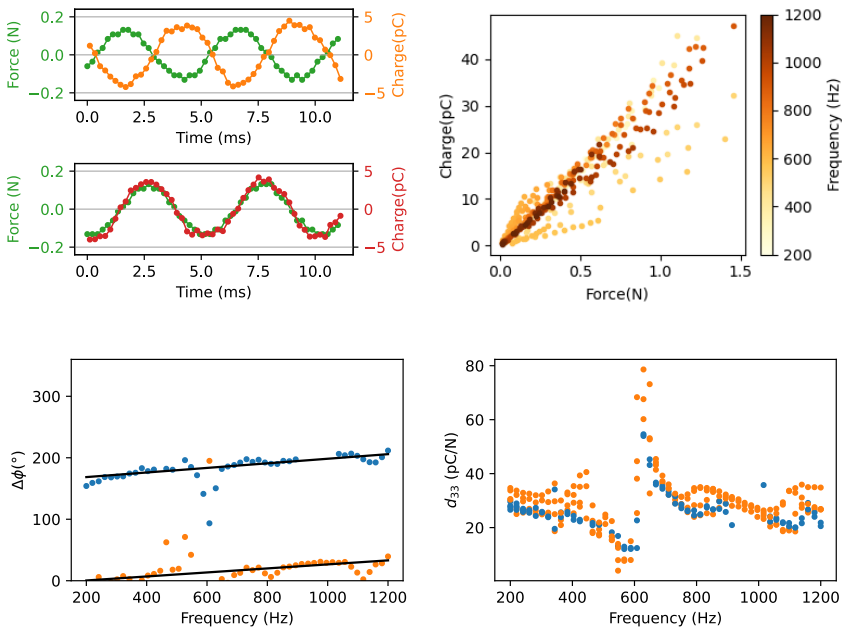

Figure 5

ha eliminato: Figure 5

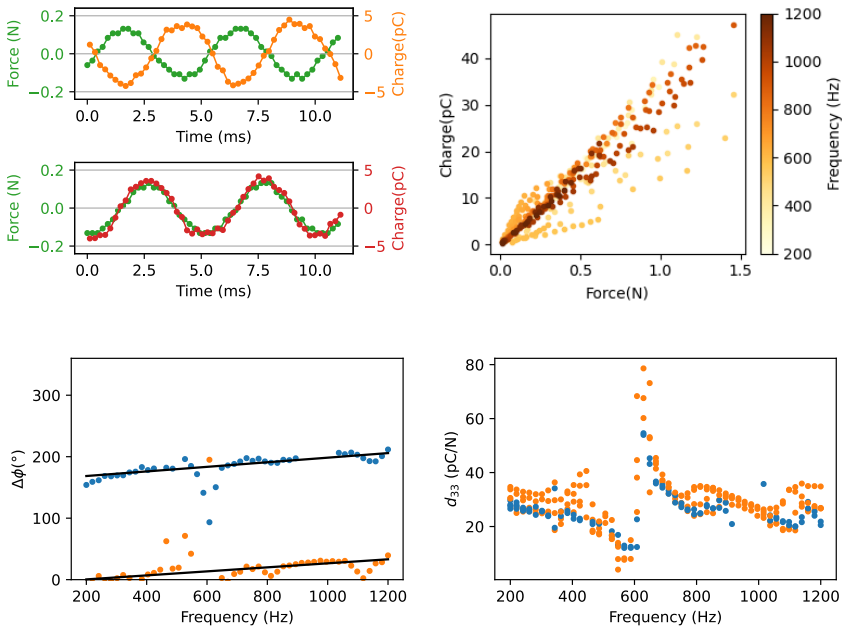

Figure 5 a) Phase inversion under sample switching for PVDF, b) Force-Charge measurement at different frequencies for a PVDF sample. c) Phase difference between the force and charge signals for the measure

in

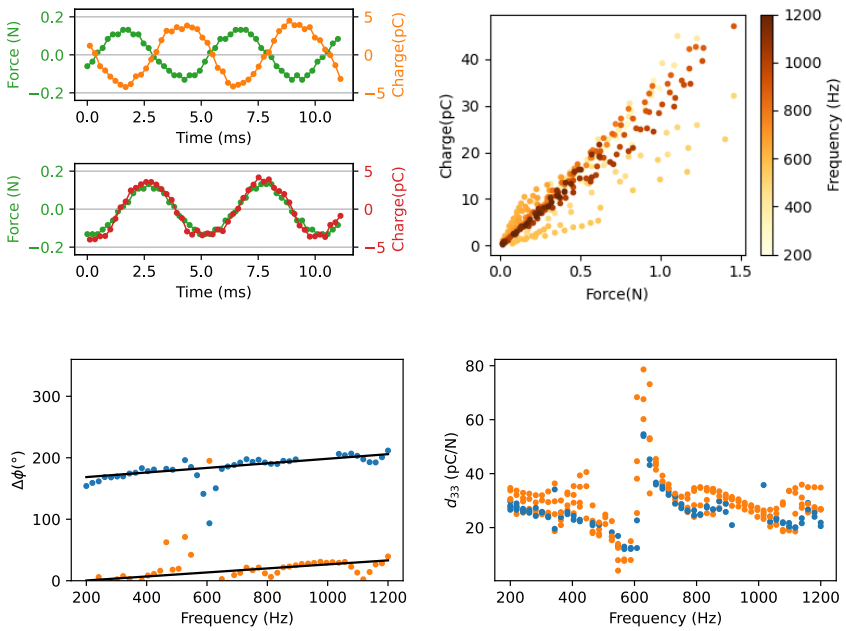

Figure 5c. The drift with increasing frequency can be ascribed to the delay between the two readings caused by the ADC clock. d) Piezoelectric coefficient spectra for PVDF in both the phase configurations. The difference between the two spectra can be ascribed to a sample anisotropy.

These measures allowed to define the measurement protocol and to identify the resonant frequencies of the instrument, at which the measures are affected by a systematic error.

The first indicator of a piezoelectric reading is the phase inversion under sample switching. The presence of this switching can only be ascribed to the anisotropic behavior of the sample, therefore it allows to exclude any other source, as for example the current induced on the electrode from the electromagnetic signal powering the exciter. The phase inversion for PVDF can be observed in In **Errore. L'origine riferimento non è stata trovata.Errore. L'origine riferimento non è stata trovata.**a, while in In **Errore. L'origine riferimento non è stata trovata.**c is plotted the phase difference between the force and charge signal for the different frequencies. As can be observed, except for some outliers and a small region around the frequency of 600Hz, the signals are definitely in phase or in counterphase, with a slight drift with increasing frequency. This drift,

ha formattato: Tipo di carattere: 11 pt, Controllo ortografia e grammatica

ha formattato: Tipo di carattere: 11 pt

ha eliminato: Figure 6

ha eliminato: Figure 6

ha eliminato: Figure 6

of roughly $7 \cdot 10^{-4}\, {}^{rad}/_{Hz}$ excluding the outliers, can be ascribed to the delay between the two signals readings, as a matter of fact since the two signals are sampled using the ADC of a single Arduino, the shift between the two readings is equal to the sampling rate of such ADC. The time delay measured from the phase drift is $\Delta t = \frac{1}{2\pi}\frac{1}{f}\frac{\partial\theta}{\partial f} = 0{,}1ms$, and the ADC of the Arduino Mega has a 9600Hz sample rate, that is converted in a 0,1ms time difference between the two measurements.

The second parameter investigated was the effect of the preload force imposed across the sample. In Figure 6 are presented some PVDF d_{33} spectra with preload forces ranging from 1N to 10N. As can be observed in the graph the spectrum is shifted down as the preload force increases, and this shifting is particularly evident for preload forces from 1 to 5N, while in the range 5-10N the signal is more stable. To analyse more accurately this behaviour, we plotted the average piezoelectric coefficient versus the preload force (Figure 6b).

ha eliminato: Figure 6

ha eliminato: Figure 6

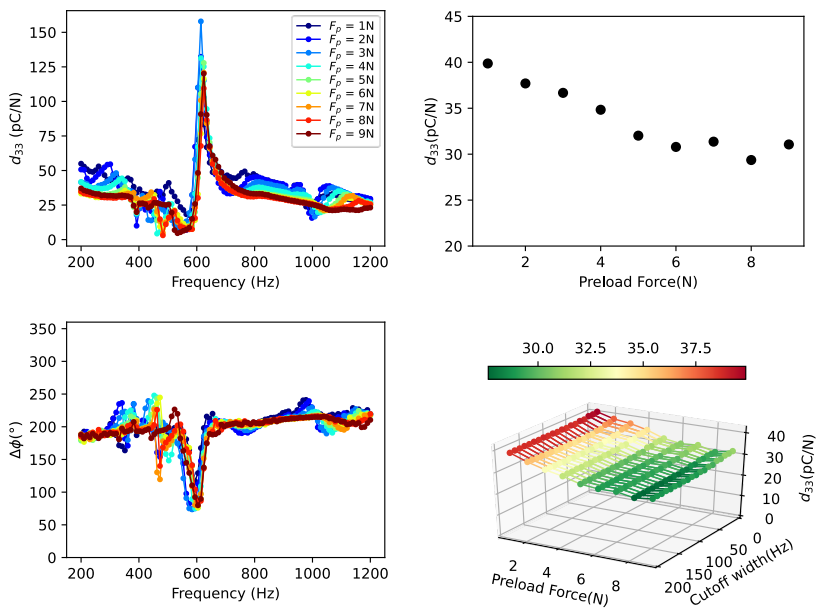

Figure 6: a) Piezoelectric coefficient spectra of PVDF with different preload forces. b) Average d_{33} of PVDF for different preload forces. In c) is represented the same, but the average is computed excluding the spike around 600Hz which is an artifact caused by a mechanical resonance of the measuring instrument.

Another observation that can be made looking at the spectra plotted in in Figure 6a is that a sharp peak of the piezoelectric coefficient around the frequency of 600Hz is present in all the measures. The peak is slightly shifted towards higher frequencies with increasing preload force and in correspondence of the peak there is a particularly high deviation from the phase difference trend discussed previously. Since all the measured samples presented this sharp peak around 600Hz, and the phase difference between the two signals is significantly far from the phase/counterphase behaviour discussed before, we inferred that this peak is an instrumental resonance and does not reflect the real electro-mechanical response of the sample. Since the d_{33} values for the frequencies around 600Hz are not relevant to our analysis we repeated the stability evaluation done in Figure 6b excluding the frequencies around 600Hz. Since we are interested in a stable and reproducible behaviour, we plot the average d_{33} coefficient with different cut-off widths (Figure 6c), and we decided to perform the measurements with a minimum preload of 5N and to ignore the frequencies between 550Hz and 650Hz.

ha eliminato: Figure 6

ha eliminato: Figure 6

ha eliminato: Figure 6

The averaged d_{33} coefficient obtained over the considered spectrum for commercial PVDF is (28,3 ± 0,3) pC/N on one side and (31,6 ± 1) pC/N on the other, which is compatible with the PVDF technical sheet (28-32pC/N). This measurement system allows to test the performance of a single side of the sample, allowing to distinguish possible anisotropies in the thickness direction of the material.

Averaging over 40 different measures made with different parameters (low forces, high forces, different feedback capacities) we obtained a mean value of (30 ± 1) pC/N.

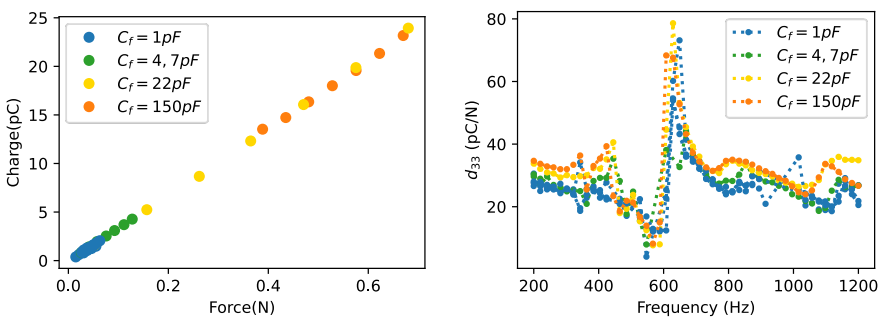

Figure 7: Force-Charge measurement (a) and piezoelectric spectra (b) of PVDF, measured using the four different gains of the instrument.

The mechanical measurements performed on the PDMS/BaTiO3-DDA nanocomposite (Figure 8a) confirmed the expected elastic behaviour for small strains (<10%) with a Young's modulus of respectively 1.70MPa and 1.57MPa for the 10%wt and 15%wt samples, which is in line with the results commonly obtained for PDMS with a base-curing agent ratio of 1:10 [26]. Compared with pristine PDMS cured at the same temperature, the nanocomposite material has a lower Young's Modulus, which represents the softening of the polymeric matrix caused by the nanoparticles embedded inside it [26]. The measures were highly repeatable, and a 100-cycles deformation measure (Figure 8b, Figure 8a c) confirmed the high mechanical stability of the material. The ultimate tensile strain of the material is respectively 121% and 125% for the 10%wt and 15%wt nanocomposite.

ha eliminato: Figure 8

ha eliminato: Figure 8

ha eliminato: Figure 8

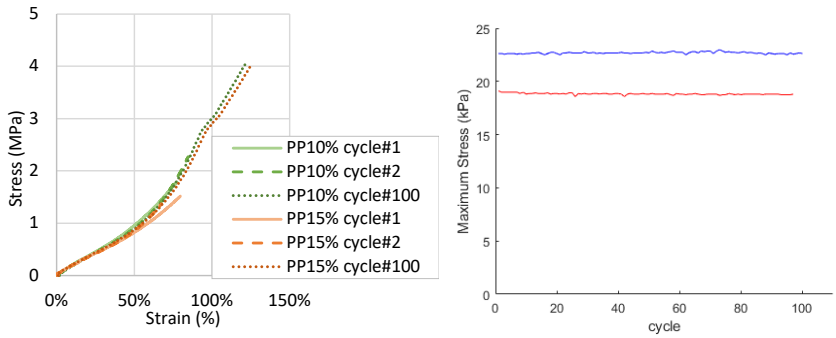

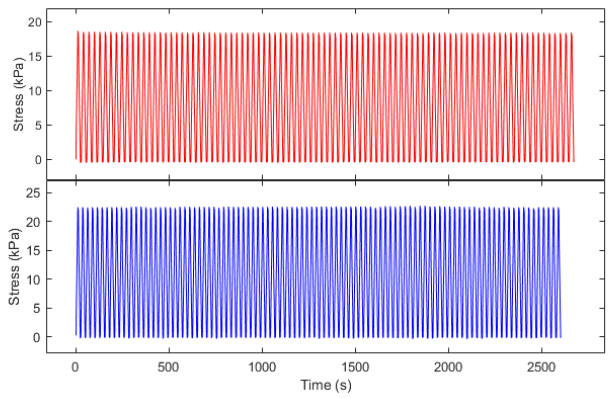

Figure 8: a) Stress-Strain measure performed over two different samples of the PDMS/$BaTiO_3$-DDA nanocomposite. The samples exhibit an elastic behavior with a Young's Modulus of respectively 1.5MPa and 1.6MPa. b)c) Mechanical stability evaluation through a100-cycle stress-strain measure. The mechanical response of the sample is stable and does not display a fatigue effect.

In Figure 9a and Figure 9b are reported the piezoelectric spectra of the different samples in both the orientation configuration. As can be observed in Figure 9 all the measures reported show a peak at 600Hz: as described before this is an instrumental resonance and does not give information about the piezoelectric behavior of the nanocomposites. In order to identify a unique piezoelectric coefficient to investigate its dependence from the nanoparticle loading and the aging or fatigue effect after a long number of cycles an average was performed between the values found at all the frequency, excluding the interval 450-650Hz, which is the frequency interval where most of the electro-mechanical cross-talk and system resonances influence the measures as discussed before.

ha eliminato: Figure 9

ha eliminato: Figure 9

ha eliminato: Figure 9

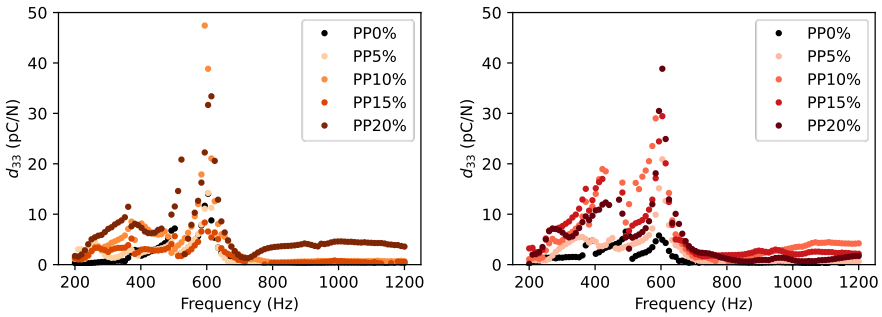

Figure 9: Piezoelectric spectra of PDMS-BaTiO3-DDA nanocomposites measured in the two configurations (same side facing up, in red, and down, in orange). The 600Hz peak is an instrumental resonance, it does not give information about the piezoelectric behavior of the nanocomposites.

In order to investigate the long-term stability of the piezoelectric effect in these samples multiple-cycle measurements were performed. In Figure 10a is shown a 10-cycle measurement for the same sample (PP15) before and after the poling procedure. As can be observed from the graphs even before the poling procedure the nanocomposite exhibits a piezoelectric behavior, but the effect is not stable, and the piezoelectric coefficient shows a 92% loss between the 1st and the 10th cycle. On the other hand, the poled sample's

ha eliminato: Figure 10

response is stable over the 10 cycles, displaying a maximum d33 variation of ±5%, depending on the tested sample. In Figure 10b is represented a 100-cycle measurement over a poled sample. The measurement lasted more than 24 hours of uninterrupted mechanical stimulation. As can be observed in the graph in Figure 10b the piezoelectric response was not significantly reduced over this span of time.

ha eliminato: Figure 10

ha eliminato: Figure 10

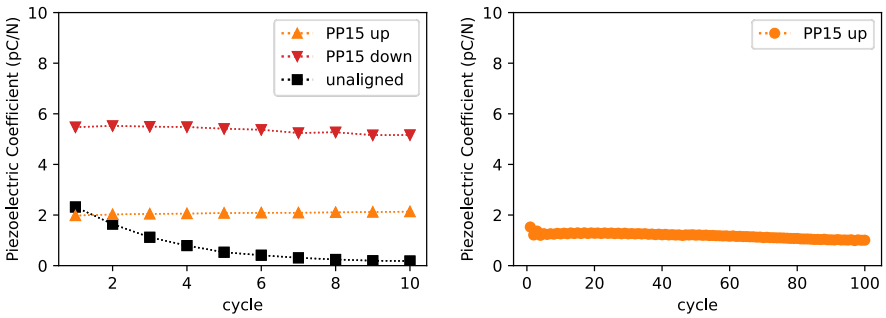

Figure 10: a) Performance loss over 10 cycles for the same sample before and after poling. During these cycles there is a 92% loss of the piezoelectric coefficient averaged across the different frequencies (excluding the peak between 400Hz and 700Hz). The measure is compared to an identical one done on the same sample gone through the poling process. b) A 100-cycle measurement over a poled sample. The measurement lasted more than 24 hours of uninterrupted mechanical stimulation. As can be observed in the graph on the right the piezoelectric response was not significantly reduced over this span of time.

In Figure 11 and Table 1 are reported the mean d_{33} values averaged over the whole spectra and at least 3 different measures. Table 1 reports also the averaged d33 percentual loss from the first to the fourth cycle as a stability evaluation. As can be observed in Figure 11d the piezoelectric coefficient increases with the nanoparticle loading in one of the two configurations, while it has a different behavior in the other. This could be ascribed to a structural anisotropy, similar to the one found in PVDF, which could be both originated by nanoparticle dispersion inside the polymer matrix and to a non-uniform poling.

ha eliminato: Figure 11

ha eliminato: Table 1

ha eliminato: Table 1

ha eliminato: Figure 11

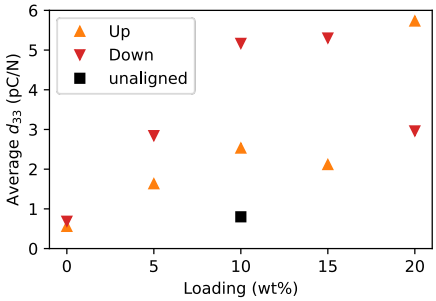

Figure 11: Mean d_{33} values averaged over the whole spectra and at least 4 separate measurements.

Table 1: Piezoelectric charge coefficients calculated averaging the piezoelectric response between the different frequencies, excluding the interval 450-650Hz where the response is highly influenced by the system resonances. Stability is represented as the averaged d_{33} percentual loss over 4 cycles.

Loading	D33 ↑ (pC/N)	D33 ↓ (pC/N)	Stability
0% wt.	0,7	0,6	-80%
5% wt.	1,6	2,8	-20%
10% wt.	5,2	2,5	-1%
15% wt.	5,3	2,1	-2%
20% wt.	5,7	3,0	-1%

In order to compare the performance this nanocomposite with the results obtained in literature some open-circuit voltage measurements were conducted using the same experimental set-up and protocol of the previous measures, by connecting the electrodes directly to the Arduino ADC converter, which has an input impedance of 20MΩ. The voltage coefficient spectra for the tested samples can be observed in

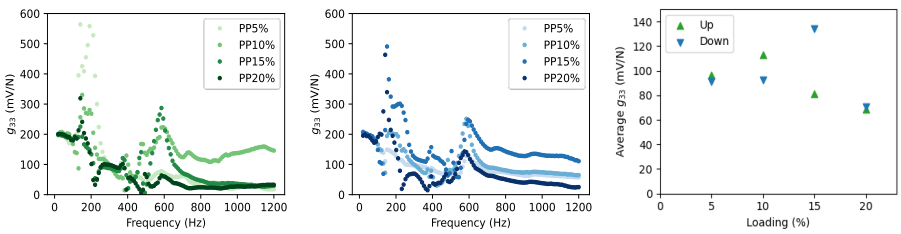

Formattato: Normale

ha formattato: Colore carattere: Automatico, Controllo ortografia e grammatica

Figure 12. Except for some mechanical resonances similar to the ones found in the charge coefficient, the samples exhibit a piezoelectric linear response between 50 and 200 mV/N depending on the stimuli frequency, with higher responses at lower frequencies (20Hz). The voltage response of the sample is not significantly influenced by the sample loading, and is comparable to the ones found in literature for similar nanocomposites [13].

ha eliminato: Figure 12

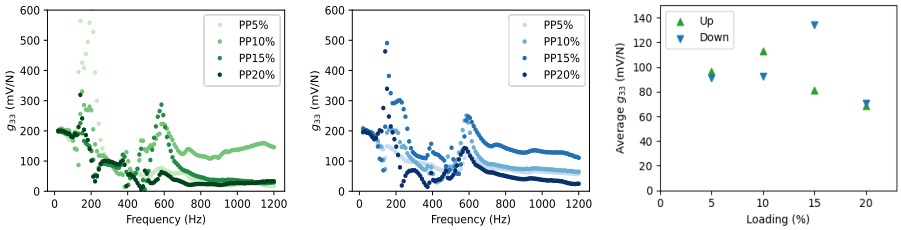

Figure 12: a) b) Open circuit voltage coefficient spectra of PDMS-BaTiO3-DDA nanocomposites, measured in the two configurations (same side facing up, in green, and down, in blue). The 600Hz peak is an instrumental resonance, it does not give information about the piezoelectric behavior of the nanocomposites. c) Mean g33 values averaged over the whole spectra.

5. Conclusions

The proposed system allows to measure both the piezoelectric coefficients spectra down to fractions of pC/N for a wide range of stimuli frequencies, and its modularity allows to expand the measurement range to higher frequencies if needed by simply substituting the various components or by developing different signal conditioning circuits for other measurement types (for example a rectifier for charge accumulation, a voltage amplifier that amplify regardless of the input impedance, etc.). The system allows to measure samples with a piezoelectric coefficient down to 0,5pC/N, and the measurements performed under controlled and reproducible conditions.

The proposed novel nanocomposite has a voltage performance in line with similar nanocomposites in literature, but has been characterized thoroughly, including charge measurement and mechanical measurements, which as stated in the introduction are critical for application purposes.

REFERENCES

[1] F. Iida and C. Laschi, "Soft robotics: Challenges and perspectives," *Procedia Comput. Sci.*, vol. 7, pp. 99–102, 2011, doi: 10.1016/j.procs.2011.12.030.

[2] T. G. Thuruthel, B. Shih, C. Laschi, and M. T. Tolley, "Soft robot perception using embedded soft sensors and recurrent neural networks," *Sci. Robot.*, vol. 4, no. 26, p. 1488, Jan. 2019, doi: 10.1126/SCIROBOTICS.AAV1488.

[3] C. Dagdeviren *et al.*, "Conformal piezoelectric energy harvesting and storage from motions of the heart, lung, and diaphragm," *Proc. Natl. Acad. Sci. U. S. A.*, vol. 111, no. 5, pp. 1927–1932, Feb. 2014, doi: 10.1073/pnas.1317233111.

[4] D. Chen and Q. Pei, "Electronic Muscles and Skins: A Review of Soft Sensors and Actuators," *Chemical Reviews*, vol. 117, no. 17. American Chemical Society, pp. 11239–11268, Sep. 13, 2017, doi: 10.1021/acs.chemrev.7b00019.

[5] Y. Qi, J. Kim, T. D. Nguyen, B. Lisko, P. K. Purohit, and M. C. McAlpine, "Enhanced piezoelectricity and stretchability in energy harvesting devices fabricated from buckled PZT ribbons," *Nano Lett.*, vol. 11, no. 3, pp. 1331–1336, 2011, doi: 10.1021/nl104412b.

[6] R. Luttmann *et al.*, "Soft sensors in bioprocessing: A status report and recommendations," *Biotechnol. J.*, vol. 7, no. 8, pp. 1040–1048, Aug. 2012, doi: 10.1002/biot.201100506.

[7] A. Kumar, "Methods and Materials for Smart Manufacturing: Additive Manufacturing, Internet of Things, Flexible Sensors and Soft Robotics," *Manuf. Lett.*, vol. 15, pp. 122–125, Jan. 2018, doi: 10.1016/j.mfglet.2017.12.014.

[8] Y. Ting, Suprapto, A. Nugraha, C. W. Chiu, and H. Gunawan, "Design and characterization of one-layer PVDF thin film for a 3D force sensor," *Sensors Actuators, A Phys.*, vol. 250, pp. 129–137, Oct. 2016, doi: 10.1016/j.sna.2016.09.025.

[9] A. Vinogradov and F. Holloway, "Electro-mechanical properties of the piezoelectric polymer PVDF," *Ferroelectrics*, vol. 226, no. 1–4, pp. 169–181, 1999, doi: 10.1080/00150199908230298.

[10] C. Zhang, P. Zhu, Y. Lin, Z. Jiao, and J. Zou, "Modular Soft Robotics: Modular Units, Connection Mechanisms, and Applications," *Adv. Intell. Syst.*, vol. 2, no. 6, p. 1900166, Jun. 2020, doi: 10.1002/aisy.201900166.

[11] L. Qian and H. Zhao, "Nanoindentation of soft biological materials," *Micromachines*, vol. 9, no. 12, 2018, doi: 10.3390/mi9120654.

[12] C. Majidi, "Soft Robotics: A Perspective—Current Trends and Prospects for the Future," *Soft Robot.*, vol. 1, no. 1, pp. 5–11, 2014, doi: 10.1089/soro.2013.0001.

[13] K. S. Ramadan, D. Sameoto, and S. Evoy, "A review of piezoelectric polymers as functional materials for electromechanical transducers," *Smart Mater. Struct.*, vol. 23, no. 3, p. 33001, 2014, doi: 10.1088/0964-1726/23/3/033001.

[14] E. K. Akdogan, M. Allahverdi, and A. Safari, "Piezoelectric composites for sensor and actuator applications," *IEEE Transactions on Ultrasonics, Ferroelectrics, and Frequency Control*, vol. 52, no. 5. pp. 746–775, May 2005, doi: 10.1109/TUFFC.2005.1503962.

[15] R. I. Mahdi and W. H. Abd Majid, "Piezoelectric and pyroelectric properties of BNT-base ternary lead-free ceramic-polymer nanocomposites under different poling conditions," *RSC Adv.*, vol. 6, no. 84, pp. 81296–81309, Aug. 2016, doi: 10.1039/c6ra12033d.

[16] J. Hillenbrand and G. M. Sessler, "Quasistatic and Dynamic Piezoelectric Coefficients of Polymer Foams and Polymer Film Systems," *IEEE Trans. Dielectr. Electr. Insul.*, vol. 11, no. 1, pp. 72–79, 2004, doi: 10.1109/TDEI.2004.1266319.

[17] A. Kachroudi, S. Basrour, L. Rufer, and al -, "Micro-structured PDMS piezoelectric enhancement through charging conditions Related content Dielectric properties modelling of cellular structures with PDMS for micro-sensor applications," 2016, doi: 10.1088/0964-1726/25/10/105027.

[18] J. Hillenbrand, Z. Xia, X. Zhang, and G. M. Sessler, "Piezoelectricity of cellular and porous polymer electrets," *Proceedings. 11th Int. Symp. Electrets*, pp. 46–49, 2002, doi: 10.1109/ISE.2002.1042940.

[19] P. Fang, L. Holländer, W. Wirges, and R. Gerhard, “Piezoelectric d33coefficients in foamed and layered polymer piezoelectrets from dynamic mechano-electrical experiments, electro-mechanical resonance spectroscopy and acoustic-transducer measurements,” *Meas. Sci. Technol.*, vol. 23, no. 3, 2012, doi: 10.1088/0957-0233/23/3/035604.

[20] K. Kim *et al.*, “3D optical printing of piezoelectric nanoparticle-polymer composite materials,” *ACS Nano*, vol. 8, no. 10, pp. 9799–9806, 2014, doi: 10.1021/nn503268f.

[21] M. Stewart and M. G. Cain, “Direct Piezoelectric Measurement: The Berlincourt Method,” Springer, Dordrecht, 2014, pp. 37–64.

[22] C.-X. Liu and J.-W. Choi, “Improved Dispersion of Carbon Nanotubes in Polymers at High Concentrations,” *Nanomaterials*, vol. 2, no. 4, pp. 329–347, 2012, doi: 10.3390/nano2040329.

[23] I. Chae, C. K. Jeong, Z. Ounaies, and S. H. Kim, “Review on Electromechanical Coupling Properties of Biomaterials,” 2018, doi: 10.1021/acsabm.8b00309.

[24] F. Galembeck, T. A. L. Burgo, L. B. S. Balestrin, R. F. Gouveia, C. A. Silva, and A. Galembeck, “Friction, tribochemistry and triboelectricity: Recent progress and perspectives,” *RSC Advances*, vol. 4, no. 109. Royal Society of Chemistry, pp. 64280–64298, 2014, doi: 10.1039/c4ra09604e.

[25] R. E. Newnham, V. Sundar, R. Yimnirun, J. Su, and Q. M. Zhang, “Electrostriction: Nonlinear electromechanical coupling in solid dielectrics,” *J. Phys. Chem. B*, vol. 101, no. 48, pp. 10141–10150, Nov. 1997, doi: 10.1021/jp971522c.

[26] I. D. Johnston, D. K. McCluskey, C. K. L. Tan, and M. C. Tracey, “Mechanical characterization of bulk Sylgard 184 for microfluidics and microengineering,” *J. Micromechanics Microengineering*, vol. 24, no. 3, p. 035017, Feb. 2014, doi: 10.1088/0960-1317/24/3/035017.